Performance comparison of Axial Flux PM machine with Anodised Aluminium Foil and Round Copper Wire

Jordi Van Damme, Hendrik Vansompel and Guillaume Crevecoeur

***Abstract*—In this article the electromagnetic and thermal performance of an axial flux permanent magnet machine with anodised aluminium foil as stator winding conductor material is analysed and compared to enamelled copper wire. The influence of the conductor material on the DC and AC winding losses, and the torque density is studied. Additionally, the influence of the motor housing convective heat transfer coefficient is examined. It can be concluded that the anodised aluminium foil winding offers an attractive alternative for copper wire, especially in low speed applications where the thermal resistance of the winding body is dominant in the thermal path from heat source to heat sink.**

***Index Terms*—Alumina, Aluminium, Aluminium-Oxide, Axial Flux, Comparison, Thermal**

I. Introduction

ANODISED aluminium foil conductor consists of aluminium foil with an electrolytically grown aluminium-oxide or alumina layer on both sides of the foil. In the past, it has already been extensively used in inductors [1], [2], transformers [3] and electromagnets [4] because of its attractive features:

- Aluminium-oxide has a high thermal conductivity (approximately 1.6 W/mK [5]) resulting in a higher equivalent thermal conductivity of the winding body [6]–[8]
- Aluminium is almost 3 times lighter than copper
- The ceramic aluminium-oxide insulation allows a higher operating temperature [9], [10]
- Aluminium has a lower price volatility and cost [11] [12]
- Aluminium windings enable an increased recyclability of an electric motor [13].
- The use of aluminium in electric motors has a lower impact on the environment compared to copper [14]

Its use in rotating electrical machines remained so far rather limited. This can have two possible explanations. First, the fact that a foil winding limits the electromagnetic design freedom and/or imposes additional manufacturing challenges. Either open slots have to be used or, removable or separated teeth are required when using (semi-)closed slots [15]. In a Yokeless and Segmented Armature (YASA) Axial Flux Permanent Magnet Synchronous machine (AFPMSM) [16] the coils can be wound before being assembled into a single stator. This overcomes the aforementioned issues opening up opportunities for innovative, highly automated manufacturing methods.

Second, the influence of anodised aluminium foil on the torque density of a rotating electrical machine is not yet completely understood. To the authors best knowledge, no rotating electrical machine using anodised aluminium foil winding was reported yet.

Note that the electrical conductivity of aluminium is 37 % lower than the conductivity of copper. Additionally, it is well known that foil windings suffer from larger AC winding losses in comparison with a conventional winding with round wire [17]–[19]. On the other hand, the higher resistivity of aluminium causes lower AC winding losses compared to an identical winding with copper conductor material [20]. Moreover, in [19] it was shown that foil windings exhibit an improved equivalent thermal conductivity compared to conventional wire windings and [6] has demonstrated a significant increase in equivalent thermal conductivity for aluminium-oxide insulated aluminium wires in comparison to enamelled copper wire. Hence, it is clear that anodised aluminium foil and enamelled copper wire have both different electromagnetic and thermal properties. In order to obtain more insight in the influence of using anodised aluminium foil on the torque density compared to enamelled copper wire both aspects have to be taken into account in a comparison. This was done in [21] for an automotive solenoid actuator, where it was concluded that the use of anodised aluminium foil allows to significantly increase the allowable solenoid current. Rotating electrical machines might also benefit from the use of anodised aluminium foil. However, due to the functional and constructional differences between solenoids and rotating electrical machines, a study specifically focusing on a rotating electrical machine is required to quantify the potential advantages of the use of anodized aluminium foil.

Motivated by the need for higher torque density in (quasi-)direct drive robotic actuators [22], the use of anodised aluminium foil conductor is considered here as an alternative to round copper wire. This paper aims to provide a comprehensive comparison between anodised aluminium foil and enamelled round copper wire used in a YASA AFPMSM

J. Van Damme was awarded a Ph.D. Fellowship Strategic Basic Research (SB) from the Research Foundation Flanders (FWO) in 2019 (Grant Number: 1S87322N).

The authors J. Van Damme, H. Vansompel and G. Crevecoeur are with the Department of Electromechanical, Systems and Metal Engineering, Ghent University, 9000 Ghent, Belgium, and with Flanders Make@UGent – EEDT-DC, 3001 Leuven, Belgium. (e-mail: jordi.vandamme@UGent.be)

designed for a (quasi-)direct-drive robotic application. This study will consider both electromagnetic and thermal aspects.

First, Section II motivates the need for higher torque density motors and prospects on how a YASA AFPMSM with anodised foil winding might be a suitable candidate to achieve this goal. The specific test case YASA AFPMSM that will be used throughout this comparative study is described. Subsequently, Section III explains how the losses are calculated that will be used as input for the thermal Finite Element Model (FEM). This model is described in Section IV and will be used to calculate the hotspot temperature of the stator. This hotspot temperature is key as it determines the allowable current and hence the maximum torque density. Finally, in Section V the losses and torque density determined in previous sections are compared for a YASA AFPMSM with either an anodised aluminium foil winding or an enamelled copper wire winding.

II. (Quasi-)direct drive YASA Axial Flux PMSM

In robotic applications such as cobots and legged mobile robots, there is the tendency to go towards low gear ratio actuators. These are called (quasi-)direct drive actuators and have a gear ratio ranging from 1:1 to 10:1 [23]. (Quasi-)direct drive actuators inherently have a higher backdrivability which enables safer, more dexterous and dynamic robots which are capable of dealing with uncertain, unstructured and changing environments [24]–[27].

Despite the attractive features offered by (quasi-)direct drive actuators they suffer from a low torque density caused by their low gear ratio, which limits the robot performance. For example, for a robot using direct-drive actuators (gear ratio 1:1) to handle a useful payload, a torque density of at least 10 Nm/kg is required which includes motor, power electronics, cooling, bearings, and housing [22], [28].

Anodised aluminium foil as conductor material can increase the torque density of the motor because of its lower mass density, its better thermal conductivity and higher allowable operating temperature. However, since aluminium has a higher resistivity and, since a foil winding has higher AC losses, it is important to take both losses and thermal properties into account when comparing anodised aluminium foil to enamelled round copper wire. To illustrate the comparison, a YASA AFPMSM motor topology was chosen because its segmented structure is inherently suited for a foil winding. Moreover, (quasi-)direct drive robotic actuators often use pancake shaped PMSMs with a short axial length [24]–[27], [29]. Having a short axial length in an axial flux machine with foil winding is beneficial in terms of AC losses, making this motor topology an interesting candidate to study the use of anodised aluminium foil conductor.

The specifications of the test case YASA AFPMSM used in the comparison study are given in Table I. The motor was designed to achieve a maximum speed of 375 rpm or 39 rad/s, which perfectly matches the speed requirements of dynamic legged robotic actuators [25]. Figure 1 gives a CAD drawing of the test case machine. Existing (quasi-)direct drive robotic actuators often use a double layer fractional slot concentrated winding [24]–[27], [29]. To provide a clear comparative study in this paper, this is also the winding type used in the test case machine.

TABLE I
Specifications of the test case YASA AFPMSM

Parameter	Symbol	Value	Unit
Number of pole pairs	N_p	13	/
Number of slots	Q_s	24	/
Number of phases	n_ph	3	/
Number of turns per tooth coil	n_turns	35	/
Maximum speed	Ω_max	375	rpm
Outer diameter stator iron core	D_o	138.5	mm
Inner diameter stator iron core	D_i	98.5	mm
Axial length stator iron core	h_stat	15	mm
Axial slot length	h_slot	10	mm
Slot width	b_slot	6	mm
Airgap thickness	h_air	1.1	mm
Magnet height	h_mag	5	mm

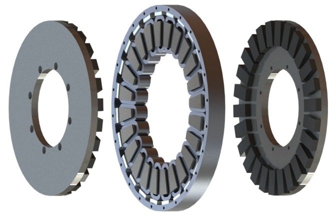

Fig. 1. CAD drawing of the test case YASA AFPMSM

III. Calculation of the Electromagnetic losses

In this section, we elaborate on the electromagnetic losses and their calculation for the YASA AFPMSM with specifications given in Table I. The stator losses can be separated in iron losses, DC and AC winding losses. These losses will be calculated using the analytical electromagnetic modelling technique for YASA AFPMSMs as elaborated in [30]. A prototype tooth coil is manufactured to experimentally determine important model parameters (Fig. 2). The rotor losses will be neglected in this study because in low speed, high torque applications the conduction losses are dominant.

A. Iron losses

The computation of the iron losses relies on the principle of loss separation. The iron losses can be written as the sum of hysteresis (P_hy), classical (P_cl) and excess loss (P_exc):

$$P_\text{Fe} = P_\text{hy} + P_\text{cl} + P_\text{exc} \tag{1}$$

Equations for the calculation of each term are elaborated on in [31], they all rely on the analytical model of the flux distribution in the stator core from [30]. The multi-slice 2D Finite Element Electromagnetic model from [31] was used to verify that no magnetic saturation occurs in the iron core. Since the iron losses are the same for the anodised aluminium foil winding and enamelled round copper wire motor, their influence on the comparison is relatively limited. Hence further details are omitted here.

B. DC Winding losses

The DC winding losses are calculated using the DC resistance R_{DC} and phase current $I_{\mathrm{ph,rms}}$.

$$P_{\mathrm{DC}} = Q_{\mathrm{s}} \cdot R_{\mathrm{DC}} \cdot I^2_{\mathrm{ph,rms}} \tag{2}$$

The DC resistance R_{DC} of a single stator coil was measured experimentally. Prototype tooth coil with both enamelled round copper wire and anodised aluminium foil were manufactured (Fig. 2). The iron core in both coils is the same. The conductor diameter of the copper wire was chosen in such a way that the slot area of both is the same. It was concluded experimentally that 35 turns of 0.9 mm copper conductor diameter resulted in approximately the same slot area as 35 turns anodised aluminium foil. A summary of the tooth coil specifications can be found in Table II.

Fig. 2. Prototype tooth coils. Left: enamelled round copper wire tooth coil, Right: anodised aluminium foil tooth coil

TABLE II
SPECIFICATIONS OF THE PROTOTYPE TOOTH COIL

Enamelled round copper wire (IEC 60317-13)	**Symbol**	**Value**	**Unit**
Outer diameter	$d_{\mathrm{Cu,o}}$	0.97	mm
Conductor diameter	$d_{\mathrm{Cu,i}}$	0.891	mm
Height laminated iron core	h_{core}	20	mm
Measured DC resistance (at 25°C)	$R_{\mathrm{DC,Cu}}$	68	mΩ
Anodised aluminium foil			
height	h_{Al}	10	mm
total thickness	$t_{\mathrm{Al,tot}}$	86	µm
thickness oxide insulation layer	t_{AlOx}	4.6	µm
Height laminated iron core	h_{core}	20	mm
Measured DC resistance (at 25°C)	$R_{\mathrm{DC,Al}}$	86	mΩ

The phase current is calculated using (assuming field orientation):

$$I_{\mathrm{ph,rms}} = \frac{T \cdot \Omega}{n_{\mathrm{ph}} \cdot E_{\mathrm{ph,rms}}} \tag{3}$$

With T, the electromagnetic torque, Ω, the mechanical rotational speed and $E_{\mathrm{ph,rms}}$ the no-load phase back emf, given by:

$$E_{\mathrm{ph,rms}} = \sqrt{2} \cdot N_{\mathrm{p}} \cdot 2\pi \cdot \Omega \cdot \xi \cdot n_{\mathrm{turns}} \frac{Q_{\mathrm{s}}}{n_{\mathrm{ph}}} \cdot \Phi \tag{4}$$

Where ξ is the fundamental winding factor, which is a product of the pitch factor ξ_p and distribution factor ξ_d as defined in [32]:

$$\xi = \xi_{\mathrm{p}} \cdot \xi_{\mathrm{d}} = \sin\left(\frac{N_{\mathrm{p}}\pi}{Q_{\mathrm{s}}}\right) \cdot \frac{\sin\left(\frac{\pi}{2n_{\mathrm{ph}}}\right)}{Q_{\mathrm{s}} \sin\left(\frac{\pi}{2n_{\mathrm{ph}}Q_{\mathrm{s}}}\right)} = 0.9468 \tag{5}$$

Φ is the peak flux linkage coupled with a single turn of a stator tooth coil, it is calculated using the equations from [30], relying on the analytical expression of the airgap flux density distribution.

C. AC Winding losses

Foil or vertical strip wound windings are known to suffer from larger AC losses than round wire windings [15]. Therefore it is important to take the AC losses into account when comparing a foil wound tooth coil with a round wire tooth coil. The calculation of the AC winding losses relies on the calculation of a resistance factor defined as the ratio of AC over DC resistance R_{AC}.

$$k_{\mathrm{R}} = \frac{R_{\mathrm{AC}}}{R_{\mathrm{DC}}} \tag{6}$$

The winding AC losses are given by:

$$P_{\mathrm{AC}} = k_{\mathrm{R}} \cdot P_{\mathrm{DC}} \tag{7}$$

The equations for the resistance factor can be found in [33]. The resistance factor depends on the number of conductors on top of each other in a slot and on the reduced conductor height ζ_{x}. For the copper tooth coil there are 3 layers of 10 and one layer of 5 conductors on top of each other. The foil winding can be considered as a single bulk conductor [17]:

$$\zeta_{\mathrm{x}} = \frac{h_{\mathrm{x}}}{\delta_{\mathrm{x}}}, \text{ with } h_{\mathrm{Al}} = 10 \text{ mm}, \; h_{\mathrm{Cu}} = d_{\mathrm{Cu,i}} = 0.891 \text{ mm} \tag{8}$$

$$\delta_{\mathrm{x}} = \sqrt{\frac{2}{\omega \cdot \mu_0 \cdot \sigma_{\mathrm{x}}}} \tag{9}$$

Where σ_{x} is the penetration depth of copper or aluminium, ω is the electrical pulsation frequency and μ_0 the magnetic permeability in vacuum.

IV. CALCULATION OF THE HOTSPOT TEMPERATURE

The torque density of the considered YASA AFPMSM, but not limited to this actuator only, is affected by the temperature limit of the stator material. Eventually, for low speed - high torque applications, conduction losses in the stator are dominant, and it was shown in [34] that the rotor temperature of a YASA AFPMSM remained well below its temperature limit.

In this case, the stator tooth coils were potted in an epoxy resin (Stycast 3050 + cat 28) with a temperature limit of 180 °C. Since this is the material in the stator with the lowest temperature limit, it is the bottleneck for the motor performance.

To determine the torque density we calculate the steady-state hotspot temperature for a certain motor operating point (torque and speed). The losses determined in Section III serve as input to the steady-state 3D thermal FEM to assess the epoxy hotspot temperature for each operating point. This temperature has to remain below 180 °C.

The thermal model development, which is briefly outlined hereafter, strongly follows the approach outlined in [35].

A. Quarter tooth coil model

Due to thermal symmetry, it is sufficient to model only one quarter of a single tooth coil. Figure 3 shows the modelled geometry. It consists of 5 different domains with different thermal properties. It is assumed that all heat is evacuated from the motor via the outer radial surface of the aluminium housing via convection. The convective heat transfer coefficient on this surface is denoted as h_{bnd}. The heat transfer via the airgap is neglected since in low speed applications the airgap convective heat transfer is low. Moreover, neglecting the airgap heatflux results in an overestimation of the hotspot temperature.

Two aluminium-oxide pads are inserted between the housing and the conductor material to guarantee sufficient electrical insulation without adding significant thermal resistance.

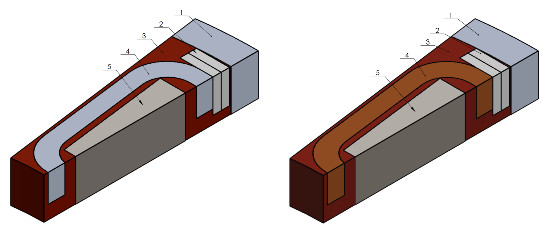

(a) (b)

Fig. 3. 3D Thermal FEM quarter tooth coil model: (1) Aluminium housing (2) Aluminium oxide thermal pad (3) Epoxy (4a) Anodised aluminium foil (4b) Enamelled round copper wire (5) Iron core

B. Anisotropic material modeling

As explained in [35], it is crucial to model the anisotropic material properties correctly. To this end, the epoxy infiltrated winding, aluminium-oxide pads and laminated iron core are modelled as homogenized material volumes in which the anisotropy is represented by a thermal conductivity tensor instead of a scalar. The winding, iron core and thermal pads have a good thermal conductivity in the direction parallel to wire strands or foil, laminations and pads respectively, and a poor thermal conductivity in the perpendicular direction.

To determine the equivalent thermal conductivity of the epoxy infiltrated anodised aluminium foil winding, a two step approach was followed. First the equivalent thermal conductivity of the anodised foil is determined, for the thermally good conducting direction using the parallel model from [6]:

$$k_{1,\text{anofol}} = f_{\text{anofol}} k_{\text{Al}} + (1 - f_{\text{anofol}}) k_{\text{AlOx,f}} \tag{10}$$

and for the thermally poor conducting direction, using the series model from [6]:

$$k_{2,\text{anofol}} = \frac{k_{\text{Al}} \cdot k_{\text{AlOx,f}}}{(1 - f_{\text{anofol}}) k_{\text{Al}} + f_{\text{anofol}} k_{\text{AlOx,f}}} \tag{11}$$

Where f_{anofol} is determined as:

$$f_{\text{anofol}} = \frac{t_{\text{Al,tot}} - 2 \cdot t_{\text{AlOx}}}{t_{\text{Al,tot}}} \tag{12}$$

In a second step, the equivalent thermal conductivities of the epoxy infiltrated anodised aluminium foil winding is determined. For the thermally good conducting direction, using the parallel model [6]:

$$k_{1,\text{Al}} = f_{\text{Al}} k_{1,\text{anofol}} + (1 - f_{\text{Al}}) k_{\text{Ep}} \tag{13}$$

and for the thermally poor conducting direction, using the series model from [6]:

$$k_{2,\text{Al}} = k_{\text{Ep}} \frac{(1 + f_{\text{Al}}) k_{2,\text{anofol}} + f_{\text{Al}} k_{\text{Ep}}}{(1 - f_{\text{Al}}) k_{2,\text{anofol}} + (2 - f_{\text{Al}}) k_{\text{Ep}}} \tag{14}$$

With f_{Al} the aluminium tooth coil winding fill factor.

The calculation of the equivalent thermal conductivities of the epoxy infiltrated aluminium-oxide thermal pads is very similar but requires only one step. It is however important to notice that a different thermal conductivity is used for the aluminium-oxide of the thermal pads and for the aluminium-oxide insulation layer on the aluminium foil. This is because the thermal conductivity of thin film alumina is different from bulk alumina [5]. Table III gives the thermal conductivities of the used materials.

TABLE III
THERMAL CONDUCTIVITY

Parameter	**Symbol**	**Value** [W/mK]
Epoxy	k_{Ep}	0.4
Aluminium	k_{Al}	235
Copper	k_{Cu}	385
Aluminium-oxide film	$k_{\text{AlOx,f}}$	1.6
Aluminium-oxide bulk	$k_{\text{AlOx,b}}$	20
Electrical steel sheet	k_{Fe}	28

The calculation of the equivalent thermal conductivities of the epoxy infiltrated copper winding and iron core is already thoroughly explained in [35]. It is therefore not repeated here.

V. Results and Conclusion of the Comparative Study

In this section, first the losses calculated according to Section III for a YASA AFPMSM with specification of Table I are given for both anodised aluminium foil and round enamelled copper wire. Then the results of the stator hotspot temperature calculation of Section IV are compared for both motors.

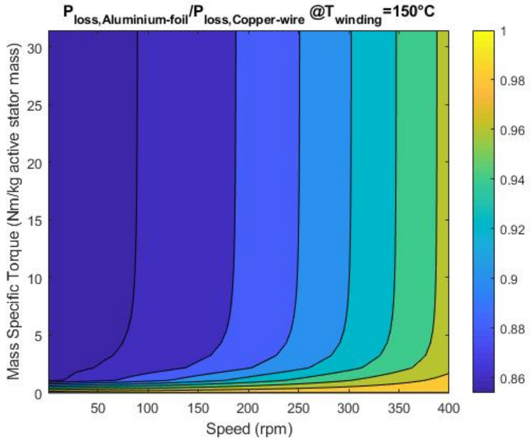

(a)

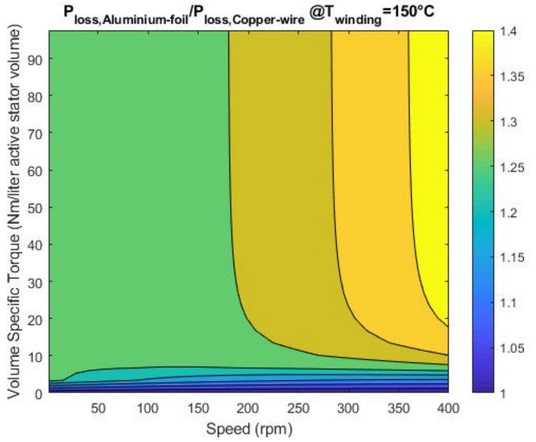

(b)

Fig. 4. Ratio of the total stator losses in an anodised aluminium foil winding over the total stator losses in an enamelled round copper wire winding: (a) mass specific torque i.e. per kg active stator mass (b) volume specific torque i.e. per liter active stator volume (c)

A. Comparison of losses

The total stator losses are the sum of the iron losses and winding losses computed in Section III. The losses are computed for a motor with anodised aluminium foil and for a motor with enamelled round copper wire, assuming the average winding temperature is 150°C. Fig. 4a shows the ratio of both losses on a mass specific basis, i.e. the torque is normalized by the active stator material mass and Fig. 4b shows the ratio on a volume specific basis, i.e. the torque is normalized by the active stator volume. From Fig. 4, it can be concluded that the anodised aluminium foil winding has lower losses on a mass specific basis over the complete torque-speed map, however the relative difference decreases for higher speeds since the AC winding losses become more dominant in the aluminium foil winding. On a volume specific basis, the enamelled round copper wire shows significantly less losses over the complete torque-speed map. This means that a prototype YASA AFPMSM with anodized aluminium foil winding will have higher losses compared to a geometrically identical motor with enamelled

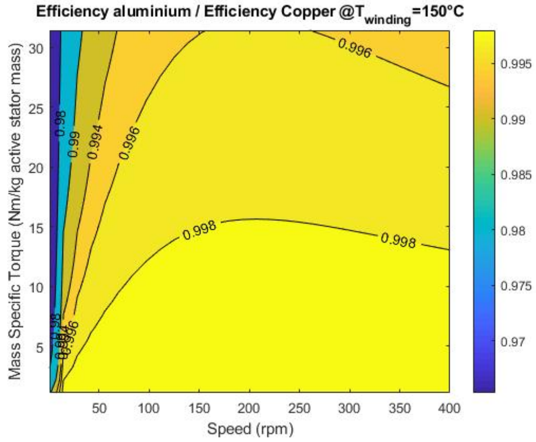

Fig. 5. Ratio of efficiency of anodised aluminium foil winding motor over efficiency of enamelled copper wire winding motor on a mass specific torque basis

round copper wire because copper has a lower resistivity, and at higher speeds the AC winding losses become more significant in a foil winding. However, as will be shown in Section V-B, this does not necessarily lead to a higher hotspot temperature and thus lower torque density. Moreover, when comparing efficiency on a mass specific torque basis, as illustrated in Fig. 5, there is only a small difference in efficiency at low speeds since in this operating area the conduction losses are dominant and these are high for aluminium due to its lower electrical conductivity. For the remainder of this Section, the results will be given on a mass specific basis.

B. Influence of housing convective heat transfer

In this Section, the influence of the convective heat flux at the boundary on the mass torque density is considered. This is done by varying the convective heat transfer coefficient at the boundary h_{bnd}. The hotspot temperature in both the anodised aluminium foil motor and enamelled copper wire motor was calculated at each torque-speed operating point using the corresponding losses given in Section V-A and the thermal FEM model from Section IV. Since both stators have a different mass, the mass normalized torque is used to compare both motors. Fig. 6a shows the ratio of the hotspot in the anodised aluminium foil winding stator over de hotspot temperature in the enamelled copper wire winding stator for a boundary convective heat transfer coefficient that is representative for a forced air-cooled housing. In Fig. 6b, the same ratio is plotted for a boundary convective heat transfer coefficient representative for a water jacket cooling. The red line and the green line connect the operating points where the maximum temperature of 180°C is reached in the copper winding and aluminium winding motor respectively. The average over the complete speed range of the mass normalized torque corresponding with this line is considered as the mass torque density of the motor. For the forced air-cooled case, the mass torque density of the anodised aluminium winding

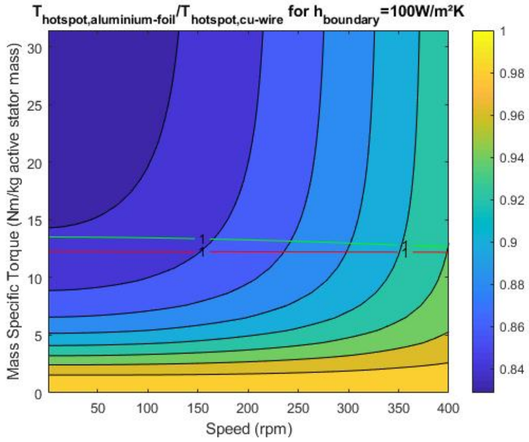

(a)

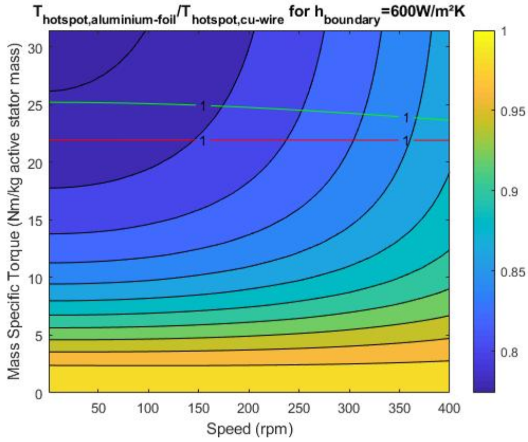

(b)

Fig. 6. Ratio of the hotspot temperature of the anodised aluminium foil winding motor over the hotspot of the enamelled round copper wire winding motor. A red line for copper and a green line for aluminium connect the operating points where the maximum temperature of 180°C is reached in steady state. (a) for a boundary convective heat transfer coefficient $h = 100W/m^2K$ (b) for a boundary convective heat transfer coefficient $h = 600W/m^2K$

is 8.5% higher. For the water jacket cooled case, the mass torque density of the aluminium winding stator is 13% higher.

Figure 7 gives the temperature difference between the aluminium and copper motor at a specific operating point (70 rpm, 12 Nm/kg active stator mass). For forced air-cooling the maximum temperature difference is 31 °C, whereas for liquid cooling the temperature difference increases up to 68 °C.

It can be concluded that under both cooling conditions, the motor with anodised aluminium foil winding exhibits a higher mass torque density. Moreover, the lower the thermal resistance to the environment, the larger the difference between anodised aluminium foil and enamelled copper wire.

C. Discussion

Keeping in mind the results from Section V-B, it can be concluded that the lower the thermal resistance between winding and environment, the more favourable the anodised

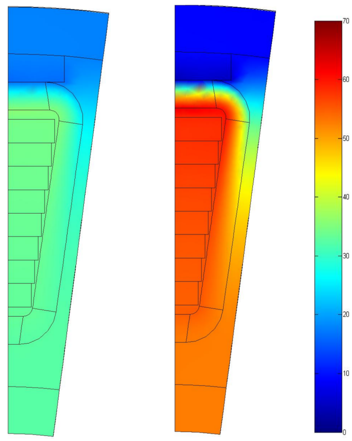

(a) (b)

Fig. 7. (a) $T_{cu} - T_{alu}$ for a boundary convective heat transfer coefficient h_{bnd} = 100 W/m²K, Ω = 70 rpm, T = 12 Nm/kg active stator material (b) $T_{cu} - T_{alu}$ for a boundary convective heat transfer coefficient h_{bnd} = 600 W/m²K, Ω = 70 rpm, T = 20 Nm/kg active stator material

aluminium foil winding is compared to the enamelled copper wire winding in terms of mass torque density. Although losses are generally higher for an aluminium winding, an anodised aluminium foil winding exhibits a lower thermal resistance. If the thermal resistance of the winding body is dominant compared to other resistances in the thermal dissipation path from heat source to heat sink, the anodised aluminium foil becomes more and more favourable in terms of mass torque density compared to enamelled copper wire. Hence, it can be concluded that anodised aluminium foil offers an attractive alternative to copper wire in (quasi-)direct drive robotic actuators.

VI. Conclusion

In this article, the use of anodised aluminium foil as conductor material in an AFPMSM is evaluated and compared in terms of stator losses and mass torque density to enamelled copper wire. It was shown that an anodised aluminium foil winding exhibits higher losses than copper wire winding but the better thermal conductivity of anodised aluminium foil winding enables a better heat dissipation resulting in up to 8.5% net higher mass torque density or 31 °C lower hotspot temperature in the case of a forced air-cooled test case AFPMSM. Additionally, it could be concluded that anodised aluminium foil winding becomes more and more favourable compared to copper wire if the winding body thermal resistance becomes the dominant factor in the heat dissipation path from heat source to heat sink. Hence, it can be concluded that anodised aluminium foil offers an attractive alternative to round copper wire in robotic application where high torque density is required.

References

[1] D. A. Hewitt, “Approaches to improving thermal performance of inductors with a view to improving power density,” 2015.

[2] H. Jordan, "Anodized aluminum foil coil with 538°c capabilities. final report," 11 1980.
[3] R. D. Carlson and R. J. Schiltz, "Power transformer for use in highly radioactive environments," 8 1961.
[4] "Applications of anodised aluminium foil." [Online]. Available: https://anofol.de/anwendungen
[5] A. Cai, L. P. Yang, J. P. Chen, T. G. Xi, S. G. Xin, and W. Wu, "Thermal conductivity of anodic alumina film at (220 to 480) k by laser flash technique," *Journal of Chemical and Engineering Data*, vol. 55, pp. 4840–4843, 11 2010.
[6] N. Simpson, R. Wrobel, and P. H. Mellor, "Estimation of equivalent thermal parameters of impregnated electrical windings," *IEEE Transactions on Industry Applications*, vol. 49, pp. 2505–2515, 11 2013.
[7] R. Wrobel, N. Simpson, P. H. Mellor, J. Goss, and D. A. Staton, "Design of a brushless pm starter generator for low-cost manufacture and a high-aspect-ratio mechanical space envelope," *IEEE Transactions on Industry Applications*, vol. 53, pp. 1038–1048, 3 2017.
[8] S. Ayat, H. Liu, M. Kulan, and R. Wrobel, "Estimation of equivalent thermal conductivity for electrical windings with high conductor fill factor." IEEE, 9 2018, pp. 6529–6536.
[9] S. Babicz, S. A. A. Djennad, and G. Velu, "Preliminary study of using anodized aluminum strip for electrical motor windings." Institute of Electrical and Electronics Engineers Inc., 12 2014, pp. 176–179.
[10] S. Babicz, S. Ait-Amar, G. Velu, A. Cavallini, and P. Mancinelli, "Behavior of anodized aluminum strip under sine and square wave voltage," *IEEE Transactions on Dielectrics and Electrical Insulation*, vol. 24, pp. 39–46, 2 2017.
[11] "Uk-alumotor research project." [Online]. Available: https://gtr.ukri.org/projects?ref=77130#/tabOverview
[12] C. R. Sullivan, "Aluminum windings and other strategies for high-frequency magnetics design in an era of high copper and energy costs." IEEE, 2 2007, pp. 78–84.
[13] J. D. Widmer, C. M. Spargo, G. J. Atkinson, and B. C. Mecrow, "Solar plane propulsion motors with precompressed aluminum stator windings," *IEEE Transactions on Energy Conversion*, vol. 29, pp. 681–688, 9 2014.
[14] A. Acquaviva, M. Diana, B. Raghuraman, L. Petersson, and S. Nategh, "Sustainability aspects of electrical machines for e-mobility applications part ii: Aluminium hairpin vs. copper hairpin." IEEE, 10 2021, pp. 1–6.
[15] P. Arumugam, T. Hamiti, and C. Gerada, "Fault tolerant winding design - a compromise between losses and fault tolerant capability," 2012, pp. 2559–2565.
[16] T. Lipo, M. Aydin, and S. Huang, "Torus concept machines: preprototyping design assessment for two major topologies," 2001, pp. 1619–1625.
[17] P. Arumugam, T. Hamiti, and C. Gerada, "Estimation of eddy current loss in semi-closed slot vertical conductor permanent magnet synchronous machines considering eddy current reaction effect," *IEEE Transactions on Magnetics*, vol. 49, pp. 5326–5335, 2013.
[18] P. Arumugam, T. Hamiti, C. Brunson, and C. Gerada, "Analysis of vertical strip wound fault-tolerant permanent magnet synchronous machines," *IEEE Transactions on Industrial Electronics*, vol. 61, pp. 1158–1168, 3 2014.
[19] M. Rios, G. Venkataramanan, A. Muetze, and H. Eickhoff, "Thermal performance modeling of foil conductor concentrated windings in electric machines," *IEEE Transactions on Industry Applications*, vol. 54, pp. 4104–4113, 9 2018.
[20] A. Selema, M. N. Ibrahim, and P. Sergeant, "Additively-manufactured ultra-light shaped-profile windings for hf electrical machines and weight-sensitive applications," *IEEE Transactions on Transportation Electrification*, pp. 1–1, 2022.
[21] L. Reissenweber, A. Stadler, J. v. Lindenfels, and J. Franke, "Improved thermal behavior of an electromagnetic linear actuator with different winding types and the influence on the complex impedance." IEEE, 12 2019, pp. 1–6.
[22] J. Hollerbach, I. Hunter, J. Lang, S. Umans, R. Sepe, E. Vaaler, and I. Garabieta, "The mcgill/mit direct drive motor project." IEEE Comput. Soc. Press, pp. 611–617.
[23] F. Ostyn, B. Vanderborght, and G. Crevecoeur, "Design and control of a quasi-direct drive robotic gripper for collision tolerant picking at high speed," *IEEE Robotics and Automation Letters*, pp. 1–8, 2022.
[24] G. Kenneally, A. De, and D. E. Koditschek, "Design principles for a family of direct-drive legged robots," *IEEE Robotics and Automation Letters*, vol. 1, pp. 900–907, 7 2016.
[25] A. Singh, N. Kashiri, and N. Tsagarakis, "Design of a quasi direct drive actuator for dynamic motions." MDPI, 11 2020, p. 8516.
[26] P. M. Wensing, A. Wang, S. Seok, D. Otten, J. Lang, and S. Kim, "Proprioceptive actuator design in the mit cheetah: Impact mitigation and high-bandwidth physical interaction for dynamic legged robots," *IEEE Transactions on Robotics*, vol. 33, pp. 509–522, 6 2017.
[27] S. Yu, T. H. Huang, X. Yang, C. Jiao, J. Yang, Y. Chen, J. Yi, and H. Su, "Quasi-direct drive actuation for a lightweight hip exoskeleton with high backdrivability and high bandwidth," *IEEE/ASME Transactions on Mechatronics*, vol. 25, pp. 1794–1802, 8 2020.
[28] "Igus rebel: Fully integrated single joint." [Online]. Available: https://www.igus.eu/info/rebel-gearbox-system
[29] H. Zhu, C. Nesler, N. Divekar, M. T. Ahmad, and R. D. Gregg, "Design and validation of a partial-assist knee orthosis with compact, backdrivable actuation." IEEE, 6 2019, pp. 917–924.
[30] H. Vansompel, P. Sergeant, and L. Dupré, "Optimized design considering the mass influence of an axial flux permanent-magnet synchronous generator with concentrated pole windings," *IEEE Transactions on Magnetics*, vol. 46, pp. 4101–4107, 12 2010.
[31] H. Vansompel, "Design of an energy efficient axial flux permanent magnet machine," 2013.
[32] K. Vogt, *Berechnung Elektrischer Machinen*. VCH, 1996.
[33] J. Pyrhönen, T. Jokinen, and V. Hrabovcová, *Design of Rotating Electrical Machines*. John Wiley and Sons Ltd, 10 2013.
[34] A. Yarantseva, H. Vansompel, and P. Sergeant, "Improvement of thermal model of an electrical machine using inverse modelling techniques," 2017.
[35] H. Vansompel, P. Leijnen, and P. Sergeant, "Multiphysics analysis of a stator construction method in yokeless and segmented armature axial flux pm machines," *IEEE Transactions on Energy Conversion*, vol. 34, pp. 139–146, 2019.

VII. Biographies

Jordi Van Damme (M'18) was born in Gent, Belgium in 1995. He received the Master degree in electromechanical engineering from the University of Ghent, Belgium in 2018. Since then, he has been with the Electrical Energy Laboratory, Ghent University, Belgium where he is currently working towards the Ph.D. degree in electromechanical engineering. In 2019, he was awarded a Ph.D fellowship from the Research Foundation-Flanders (FWO). His current research interests include the design and control of integrated modular electric actuators for mechatronic applications.

Hendrik Vansompel was born in Belgium in 1986. He received the MSc and PhD degrees in electromechanical engineering from Ghent University, Ghent, Belgium, in 2009 and 2013, respectively. He is currently a Postdoctoral Research Assistant with the Department of Electromechanical, Systems and Metal Engineering, Ghent University. His research interests include electric machines and power electronics.

Guillaume Crevecoeur received the M.Sc. and Ph.D. degrees from Ghent University, Ghent, Belgium, in 2004 and 2009, respectively, both in engineering physics. Since 2014, he is appointed as an Associate Professor at the Department of Electromechanical, Systems and Metal Engineering of Ghent University. With his team, he conducts research at the intersection of system identification, control and machine learning for mechatronic and industrial robotic systems. Prof. Crevecoeur is also an affiliate member of Flanders Make, the strategic research center for the manufacturing industry in Flanders, Belgium